Nanomechanical Plasmon Spectroscopy of Single Gold Nanoparticles

Daniel Ramos[a], Oscar Malvar[a], Zachary J. Davis[b], Javier Tamayo[a], and Montserrat Calleja[a]

[a]Bionanomechanics Lab, Instituto de Micro y Nanotecnología, IMN-CNM (CSIC), Isaac Newton 8 (PTM), E-28760 Tres Cantos, Madrid, Spain. [b] Danish Technological Institute, Gregersensvej 1, 2630 Taastrup, Denmark.

We experimentally demonstrate the effect of the localized surface plasmon resonance (LSPR) of a single gold nanoparticle (AuNP) of 100 nm in diameter on the mechanical resonance frequency of a free-standing silicon nitride membrane by means of optomechanical transduction. We discover that a key effect to explain the coupling in these systems is the extinction cross section enhancement due to the excitation of the LSPR at selected wavelengths. In order to validate this coupling we have developed a fixed wavelength interferometric readout system with an integrated tunable laser source, which allows us to perform the first experimental demonstration of nanomechanical spectroscopy of deposited AuNPs onto the membrane, discerning in between single particles and dimers by the mechanical frequency shift. We have also introduced three-axis mechanical scanners with nanometer-scale resolution in our experimental setup to selectively study single nanoparticles or small clusters. Whereas the single particles are polarization-insensitive, the gold dimers have a clearly defined polarization angle dependency as expected by theory. Finally, we found an unexpected long-distance (~200 nm) coupling of the LSPR of separated AuNPs coming out from the guided light by the silicon nitride membrane.

Keywords: Optomechanics, gold nanoparticles, plasmon coupling, nanomechanical spectroscopy

Researchers have long held interest in translating electromagnetic energy into mechanical motion, being the first proposed optomechanical effect introduced by Kepler to explain the deflection of comet tails away from the sun at the end of sixteenth century. Nowadays, the prospect of observing quantum phenomena in mesoscopic mechanical systems[1] has motivated a reemerged interest in optomechanical systems, whose canonical image is an optical cavity in which one, or both, of the fixed mirrors is substituted by a freely moving reflecting resonator[2]. In this case, the trapped photons inside the optical cavity act on the mechanical behavior of the resonator mainly by means of direct moment exchange[3] or through the photothermal effect[4, 5]. Long-time pursued milestones like single photon occupation or minimization of the mechanical energy loss in self-oscillation regime have been achieved by taking advantage of the raised optomechanical coupling. These achievements can be exploited for ultrasensitive detection of force[6] and/or mass in sensing schemes[7] and scanning probe applications[8]. According to previous studies in literature, the optomechanical coupling is dramatically improved by using high-Q cavities, being the photonic crystal cavities

the more promising candidates to reach the largely pursued quantum regime in mesoscopic mechanical resonators[9]. However, in this work we are using an orthogonal approach that departs from the cavity optomechanics by means of plasmonic systems, which are the unique systems that can truly confine light at the nanoscale. Plasmonic systems offer an interesting route to explore optomechanical coupling without the need of high-Q optical cavities.

Despite the low-quality optical factor exhibited by the broad optical resonances, plasmomechanical systems represent an attractive alternative when compared with other optical cavities in literature because the localized plasmon resonances[10-12] (LPR) are easily excited by free-space light beams[13]. This issue is of crucial importance because the free-space optomechanical coupling largely decays when the size of the mechanical system is below the wavelength[14], which, on the other hand, it is needed to achieve high frequency regime. Researchers have dealt with the diffraction limit by engineering optical resonators operating in telecom wavelengths or by using the scattered electromagnetic field to apply the feedback force on the mechanical resonator[15].

Here, we demonstrate the optomechanical coupling that emerges in the low finesse plasmonic cavity formed by a spherical gold nanoparticle of 100 nm in diameter onto a free-standing silicon nitride membrane. We discover that a key effect to explain the unexpected optomechanical coupling in these systems is the excitation of the plasmon resonance which is related with an enhancement in the extinction cross section of the nanoparticle at a selected wavelength. The extinction is the combination of the absorption and the scattering of the particle, therefore the particle becomes a hot spot on the mechanical membrane consequently tuning the mechanical resonance frequency through thermomechanical effects. As it is known in literature, the plasmon resonance can be controlled by different methods like the change of the particle diameter or by clustering the particles[16, 17], which allows the harnessing of the collective plasmonic modes. This cluster coupling usually vanishes when the separation between the particles exceeds the exponentially decreasing distance in which the evanescent field expands, which usually is in the order of few nanometers. However, we demonstrate the use of a membrane to efficiently extend the range of applicability of the coupling between nanoparticles to hundreds of nanometers. This is achieved by means of the evanescent field guiding accomplished by the silicon nitride membrane.

In this work, we have investigated the optomechanical behavior of suspended silicon nitride membranes[18]. The membrane was defined by patterning a series of holes (on a square lattice) onto a silicon nitride layer and the subsequent wet etch of the underneath silicon dioxide layer. The stochastic Brownian vibration of the membranes was measured by a homemade optical interferometer, Fig. 1a. The addition of a computer controlled 3D scanner allows the simultaneous acquisition of the static deflection of the membrane and the shape of any vibration mode of our choice with picometer range displacement sensitivity in vibration amplitude and a nanometer scale resolution in lateral displacement. This is achieved by analyzing the two components of the reflectivity: the DC signal, which is used for the static deflection; and the AC component of the signal for the vibrational modes. The nominal length, width and thickness of these membranes are respectively 50μm, 50μm and 150nm with an

internal stress of about 927 MPa, being the fundamental resonant mode of about 8.6 MHz. Fig. 1b-g shows a modal analysis (vibration amplitude at resonance at different positions) for the first six mechanical modes. Each experimental amplitude map consists of ten times averaged 512x512 individual measurements, giving as a result $1.6x10^7$ (10x512x512x6) acquired mechanical spectra. The measurements were performed in high vacuum conditions ($\sim10^{-7}$mbar) where the mechanical quality factor for the fundamental mode is of ~17000. This high value for the mechanical quality factor is in good agreement with the values reported in literature for stressed structures[19].

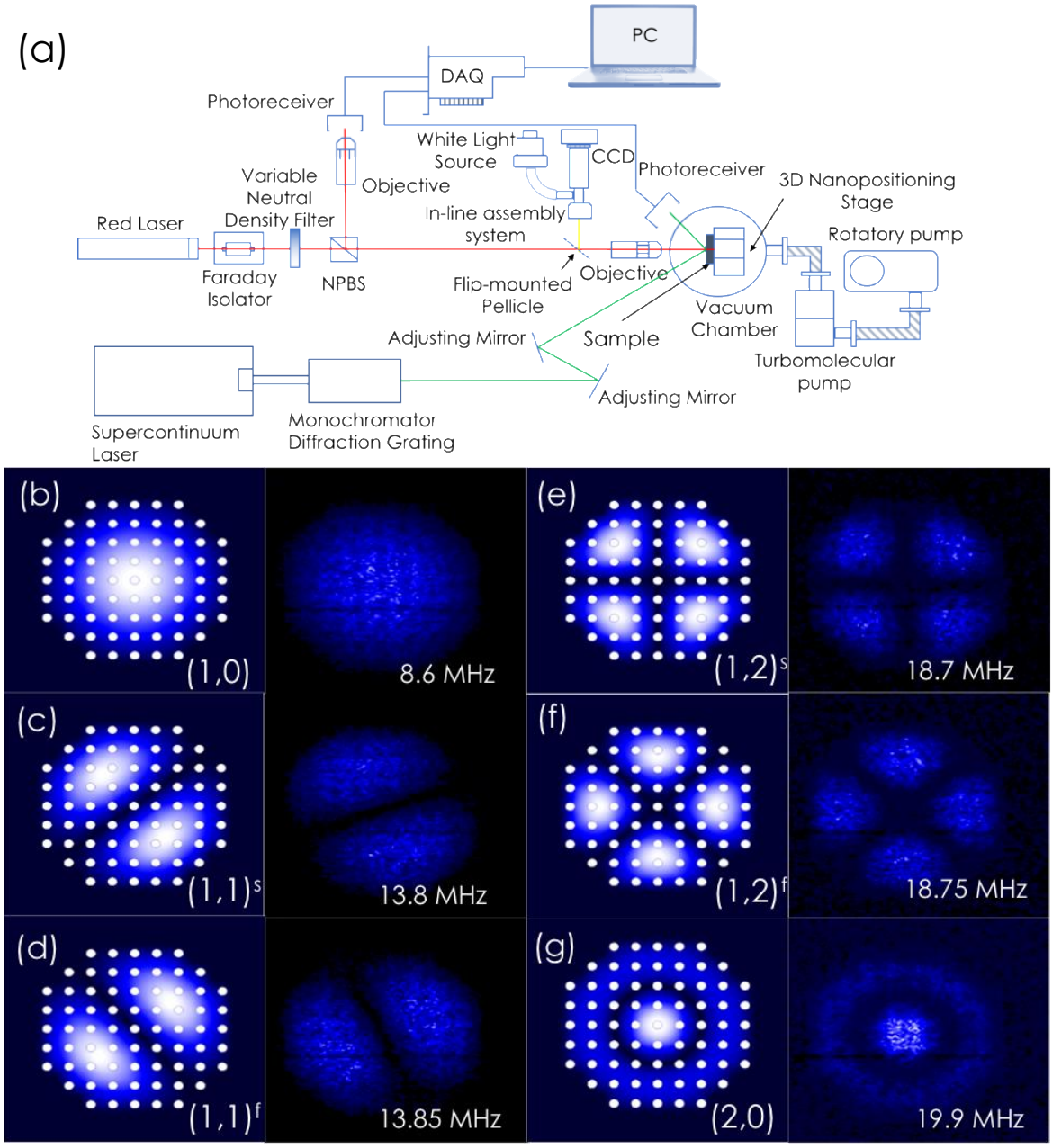

Figure 1. Mechanical mode profile. a. Schematics of the experimental setup for optomechanical characterization of free-standing membranes. **b-g.** Finite element simulations (left) and experimental measurements (right) of the amplitude of the first six mechanical modes for the membranes under study. The color contour plots show the amplitude of the mode measured by scanning the sample. The label on the FEM simulations represents the mode, whereas the label on the measurement is the experimental frequency. The modes are labeled as $(m,n)^i$, where m and n represents respectively the number of radial and angular nodes and the subscript $i = s,f$ stands for "slow" or "fast" attending to the frequency of the degenerated modes.

The full width at high maximum (FWHM) is of about 100 Hz, which allows to spectrally resolve the different mechanical modes, even the "degenerated" ones (the degeneration is broken due to the stress and fabrication imperfections), marked in the figure with the super-indices *s* and *f* for "slow" or low frequency and "fast" or high frequency.

Therefore, we are able to measure spatially resolved mechanical spectra. By using this technique, we can study the local effect of single nanoparticles. We have deposited 100 nm diameter gold nanoparticles onto the suspended membranes by using a homemade electrospray chamber[20]. This system comprises three different stages with decreasing pressure. At the first stage, an ESI (electrospray ionization) unit is used to generate mostly desolvated charged species at ambient pressure. The charged species are immediately attracted by the second stage, a heated metallic capillary at 200 ºC and vacuum pressure (~10 mbar) placed at 5 mm below the ESI needle. The high temperature is necessary to fully desolvate the microdroplets and to prevent analyte loss by sticking to the internal wall of the capillary. The charged particles at the exit of the heated capillary are attracted by a skimmer with a 100 μm wide orifice that connects with the third stage, a low vacuum chamber (~0.1 mbar) in which the membranes are placed a few centimeters below the hole.

The high efficiency of the ESI technique allows to work at very low nanoparticles' concentration, which assures to have single nanoparticles landing on the membrane, Fig. 2a. The monodispersed gold nanoparticles (less than 12% of variability in size and shape, Sigma-Aldrich) have a diameter of 100 nm, which means a mass of 10^{-17} kg

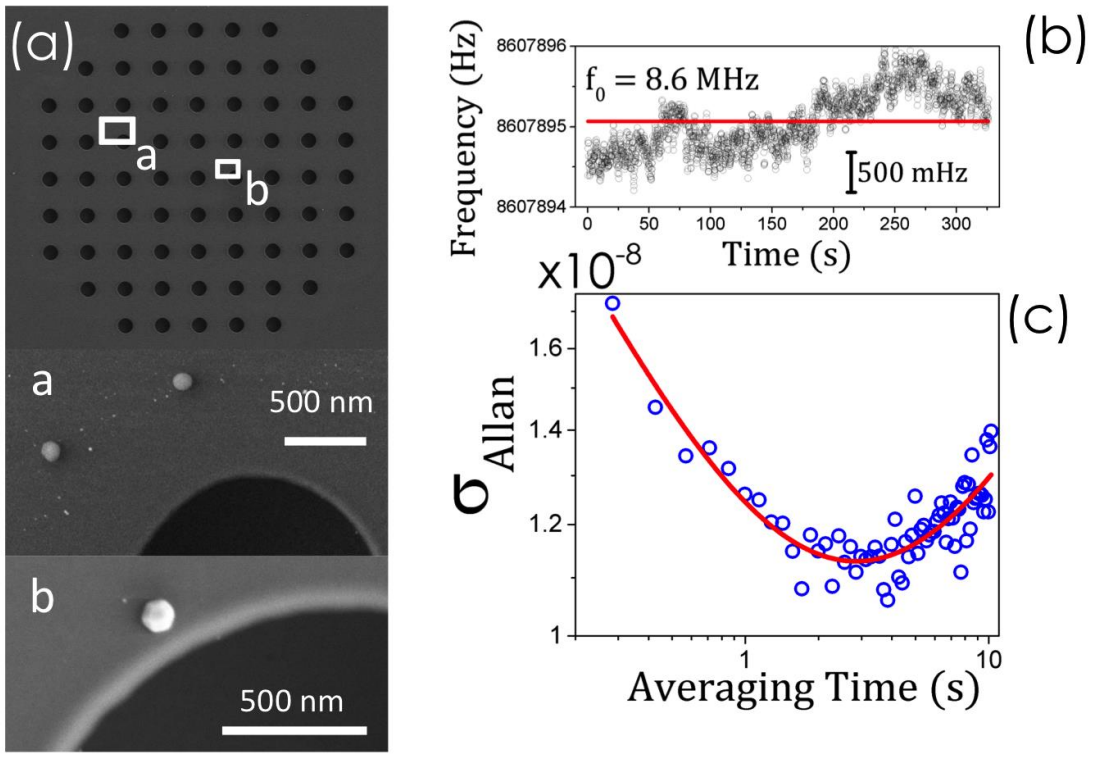

Figure 2. Mechanical characterization. a. Scanning electron microscope images of a representative silicon nitride membrane. Labels *a* and *b* indicate the landing site of gold nanoparticles, the zoom images show a group of two nanoparticles in *a* and a single nanoparticle *b*. **b.** Experimental measurement of the fundamental resonance frequency of the membrane as a function of time. The measurement shows a noise level of about 500mHz. **c.** Allan deviation of the fundamental resonance mode of the measured membrane reaching a value of 10^{-8} for integration times of about 2-3 s the red solid line is just a guide for the eye.

The experimental measurements were performed using a homemade optical system[18] with two lasers in the visible range: a red laser (5 mW, 633 nm, Thorlabs, Inc.), and a green laser (3 mW, 543 nm, Edmund Optics Ltd.). The laser beam is focused on the sample by means of a long working distance Mitutoyo objective (50X, NA 0.55) that reaches a spot size of 1.8 μm. The sample containing the suspended membranes is held in a high vacuum environment (10^{-7} mbar). In order to reach those conditions, a high vacuum chamber is pumped down by means of a rotatory and a turbomolecular pump (Varian, Inc.). Backscattering reflections could damage the laser; therefore, a Faraday isolator cell has been introduced within the light path. By tracking the resonance frequency as a function of the time, we observe a frequency noise of about 500mHz for time intervals of few minutes, Fig. 2b. The way to characterize the noise level of our readout system is to calculate the Allan deviation, $\sigma_{Allan}(\tau) = \sqrt{{\sigma_{Allan}}^2(\tau)}$, where ${\sigma_{Allan}}^2(\tau)$ is defined as the Allan variance and it is calculated from the average of frequency samples measured in a temporal integration time τ, ${\sigma_{Allan}}^2(\tau) = {}^1/_2 \langle \left(\bar{f}(t +$

$1) - \bar{f}(t)\Big)^2\rangle$. The Allan deviation reaches a value of 1.1×10^{-8} for an integration time of 3s, Fig.2c.

The inertial mass of the membrane is of about 3.4×10^{-12} kg, which means that, by using the simplified point mass model, a single gold nanoparticle of 100nm in diameter induces a relative frequency downshift of about 1.5×10^{-5}. This value is, in principle, above our frequency noise level and it could be detected in an *in situ* mass sensing experiment. However, for *ex situ* measurements it is really hard to detect such small frequency changes due to thermal and/or mechanical drifts. Therefore, if we are interested in single particle detection, we have to develop different sensing strategies.

By using the mechanical sweep method described above, it is possible also to make a frequency map, this is the frequency measured at each laser focusing point on the silicon nitride membrane, Fig. 3a. Although the vibration amplitude is not the same along the membrane, following the eigenmode shape, the frequency should be constant over the whole resonator. This is not what we find experimentally, as it can be clearly seen from Fig. 3a, where there are darker areas in the color map, indicating a frequency change. An scanning electron microscope inspection of the sample, as seen in Fig. 2a, reveals that the low frequency points corresponds to the nanoparticles landing sites. This effect is caused by the localized surface plasmon resonance LSPR excitation produced by the laser while scanning the resonator surface to create the map[11]. When the laser spot excites the LSPR of the nanoparticle, the absorption cross section increases, which produces a local heating or "hot spot", consequently changing the resonance frequency, (Fig. 3b-c). Figure 3b shows the temperature profile calculated by FEM simulations by considering a hot spot at the position in a Fig. 2a for different absorption powers ranging from 10 nW to 10 μW. The simulations take into account that the membrane is placed at high vacuum and there is no convection, the only heat transfer mechanism is radiation (which is negligible for this configuration) and conduction to the heat sink (the silicon layer). This temperature profile is translated into a frequency shift by means of both the non-released stress generated in the structure due to the thermal expansion and the temperature dependency of the Young's modulus of the material. Both mechanisms have been taken into account in multiphysics simulations shown in Fig. 3c.

By taking into account the simulated sensitivity of the structure, Fig.3c, for an integration time of about 3s, we have an Allan variance of 1.1×10^{-8}, which means that the noise of our fundamental mechanical resonance at 8.6MHz is of 95mHz. Therefore, the minimum detectable power is 72pW. On the other hand, the state-of-the-art commercially available photodetectors (e.g. Si biased photodetector) have a typical dark current at room temperature of about 1nA and a responsivity at 632nm of ~0.45A/W which means that the minimum power they can detect is 2.2nW. Therefore, the proposed optomechanical device is two orders of magnitude more sensitive than a commercially available photodetector.

In this frequency map we can easily distinguish two different values of the resonance frequency drop, these points were labeled as "single" and "dimer" gold nanoparticles.

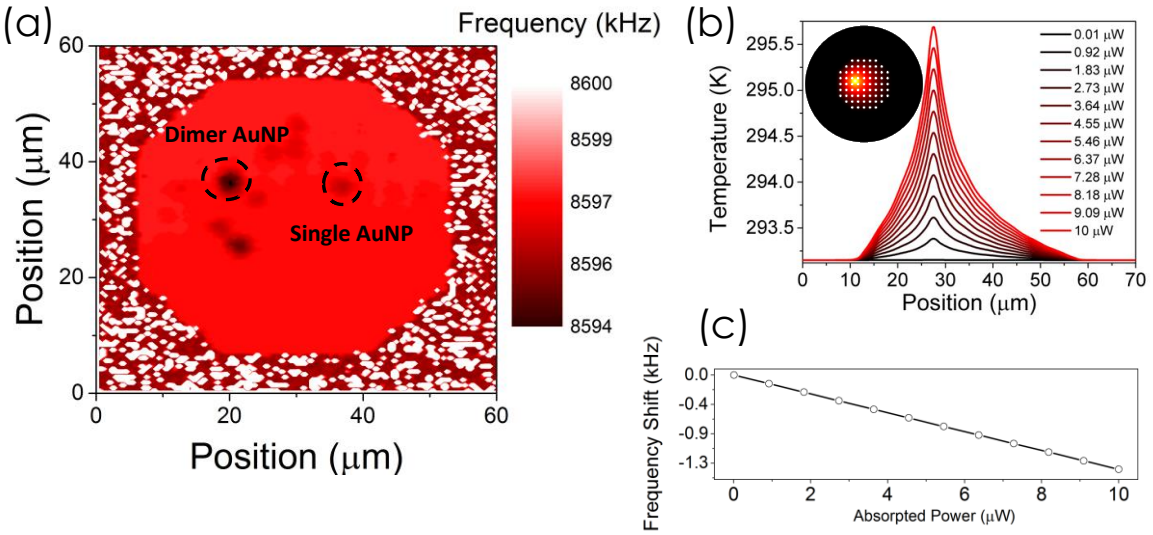

Figure 3. Physical mechanism of frequency shift variation. a. Experimental frequency map obtained by the mechanical sweeping technique. Each frequency drop appears as a dark area in this map, distinguishing two different families labeled as dimer and single gold nanoparticle according to SEM inspection. **b.** Simulated temperature profile of the silicon nitride membrane due to the light absorption at position labeled as "dimer AuNP" in the experimental frequency map. Inset shows a color map of the temperature distribution across the whole structure. **c.** Simulated frequency shift due to the presence of the hot spot simulated in b. Inset shows the mode profile simulated of the fundamental mechanical mode

The nanoparticle clusters, i.e. the gold dimers, define two axis, one aligned to the particles and the perpendicular one, Fig. 4a. Therefore, it is possible to analyze the frequency shift as a function of the polarization angle by taking as a reference the axis of the dimer, Fig. 4b. Blue line in figure 4b represents the frequency as a function of the polarization angle while shining out of the nanoparticle cluster, showing negligible frequency shift as expected. Red line represents the frequency shift as result of the change in the polarization of the laser shining the cluster. As it can be seen from the measurements, there are three differentiated angular regions: from zero to approximately 50 deg, where the resonance frequency shift of the fundamental mode decreases about 2 kHz; the second region ranges from 50 to 130 deg, where the resonance frequency shift is of about -1.6 kHz; and finally from 130 to 180 deg, where the frequency shift recovers the value of -2 kHz. This is in very good agreement with the previously published data in literature[21, 22]. We have also checked this behavior by mechanically sweeping the sample at different polarization angles ranging from 90 degrees to 180 degrees respect to the dimer axis. Note that the waist of the laser spot is of about 1.8 μm, therefore, we have enough spatial resolution to probe the nanoparticles. These frequency shifts are at least two orders of magnitude larger than the expected ones in a mass sensing experiment.

This device can be used as part of a nanomechanical spectroscopy technique by simply shinning the whole membrane with a tunable wavelength source[18] while

measuring the resonance frequency of the fundamental mechanical mode by using a red laser at the middle point of the membrane. Since we are shinning the whole membrane, we are exciting at the same time both the single particles and the dimer clusters showed in Fig. 3 (a). Therefore, according to the electric field distribution resulting from finite element simulations of single and dimer gold nanoparticles, we expect two maxima in absorption corresponding to the enhancement of the extinction cross section of single and dimer gold nanoparticles, blue and red lines respectively in Fig. 4(d). These spectra were obtained by focusing the tunable laser only on positions a and b labeled in Fig. 2. The measured resonance frequency, black line in Fig. 4(e), decreases at the position of the localized plasmon resonance of a gold nanoparticle on a 140nm thick silicon nitride surface, with a shift of ~530 nm for the single particle and of ~610 nm for the dimer cluster. The observed noise in this experimental measurements could be understood as the convolution of the stochastic mechanical noise with an undesired Fabry-Perot cavity sustained by membrane-substrate separation or the optical components. According to the experimental measurements gold nanoparticles exhibit a collective behavior even at large separation distances always below the illuminating spot size. In this particular case, the measured nanocluster separation is of about 500nm. This is attributed to an additional coupling by means of the light guided by the 140 nm thick silicon nitride membrane, which is confirmed by simulations of the extinction cross section, either in vacuum or in contact with the membrane.

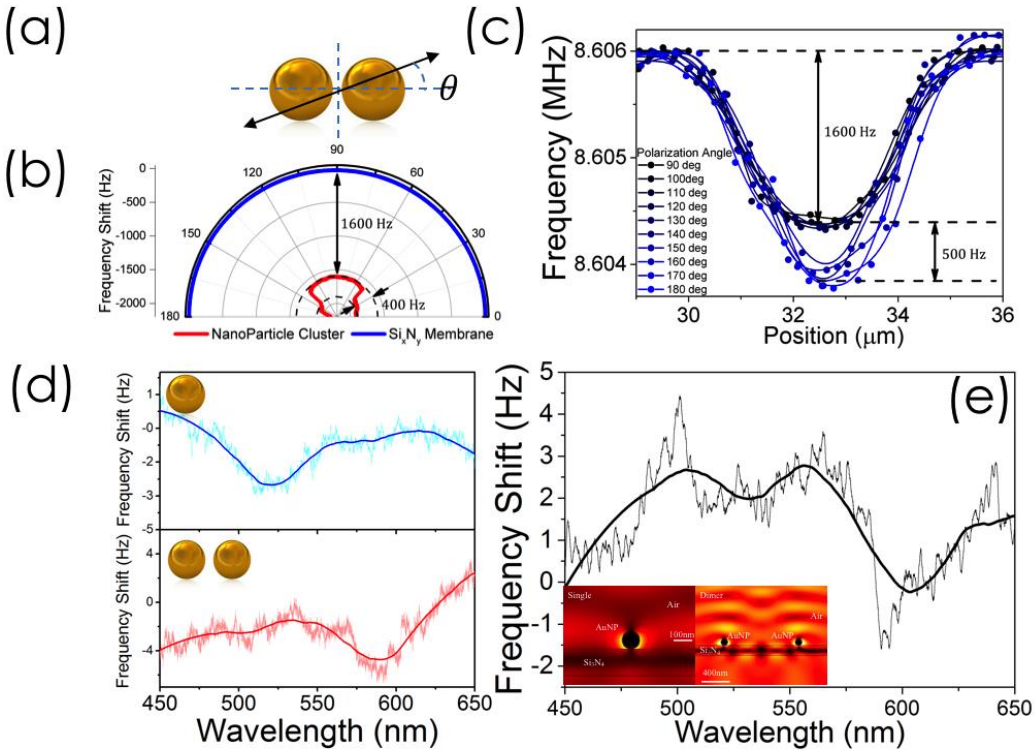

Figure 4. Nanomechanical Spectroscopy. a. Schematic representation of the nanoparticle dimers under study. **b.** Experimental measurement of the frequency shift as a function of the polarization angle on the membrane (blue curve) and on the nanoparticle dimer (red curve). **c.** Experimental measurement of the resonance frequency of the

membrane while scanning across the nanoparticle dimer for different polarization angles ranging from 90 degrees (perpendicular to the dimer axis) to 180 (parallel to the dimer axis). **d.** Nanomechanical spectroscopy of a single gold nanoparticle (blue curve) and a dimer (red curve). **e.** Nanomechanical spectroscopy of the membrane with two types of plasmonic particles: single particles and dimers.

In conclusion, we demonstrate the nanomechanical spectroscopy of single gold nanoparticles and dimers coupled to a suspended silicon nitride membrane and the mapping of frequency shift of the resonance frequency of the fundamental mechanical mode of the membrane. For a fixed laser wavelength, the polarization-dependent absorption is related with the symmetry axis of the dimer. By shining the whole membrane with a tunable wavelength source we are able to discern in between the effect of single or dimer nanoparticles attending the position of the absorption maxima. We have both theoretically and experimentally demonstrated that the frequency shift is a consequence of local heating; therefore, both, single or dimer nanoparticles, can be independently studied on the same membrane by simply focusing the tunable laser on the area containing the clusters of interest. Our results show that nanomechanical resonators are a unique and robust tool for probing plasmonic nanostructures, and they can be used as a platform of new kind of applications like for example, mechanical based photodetectors or pico-calorimeters for heat exchange tracking of biochemical reactions and/or probing thermal properties of nanoscale structures.

AUTHOR INFORMATION

Corresponding Author

*E-mail: daniel.ramos@csic.es

ORCID

Daniel Ramos: 0000-0003-2677-4058

Author Contributions

The manuscript was written through the contributions of all authors. All authors have given approval to the final version of the manuscript.

Notes

The authors declare no competing financial interest.

ACKNOWLEDGMENTS

This work was supported by the Spanish Science Ministry (MINECO) through project TEC2017-89765-R and by the European Union's Horizon 2020 research and innovation program under grant agreement No 731868–VIRUSCAN and European Research Council grant 681275 – LIQUIDMASS- ERC- CoG-2015. D.R. acknowledges the RyC fellowship supported by MINECO. All authors acknowledge the service from the X-SEM Laboratory at IMN and funding from MINECO under project CSIC13-4E-1794 with support from EU (FEDER, FSE).

References

1. O'Connell, A. D.; Hofheinz, M.; Ansmann, M.; Bialczak, R. C.; Lenander, M.; Lucero, E.; Neeley, M.; Sank, D.; Wang, H.; Weides, M.; Wenner, J.; Martinis, J. M.; Cleland, A. N. *Nature* **2010,** 464, 697.
2. Aspelmeyer, M.; Kippenberg, T. J.; Marquardt, F. *Reviews of Modern Physics* **2014,** 86, (4), 1391-1452.
3. Anetsberger, G.; Arcizet, O.; Unterreithmeier, Q. P.; Rivière, R.; Schliesser, A.; Weig, E. M.; Kotthaus, J. P.; Kippenberg, T. J. *Nature Physics* **2009,** 5, 909.
4. Metzger, C. H.; Karrai, K. *Nature* **2004,** 432, 1002.
5. Ramos, D.; Gil-Santos, E.; Pini, V.; Llorens, J. M.; Fernández-Regúlez, M.; San Paulo, Á.; Calleja, M.; Tamayo, J. *Nano Letters* **2012,** 12, (2), 932-937.
6. Gloppe, A.; Verlot, P.; Dupont-Ferrier, E.; Siria, A.; Poncharal, P.; Bachelier, G.; Vincent, P.; Arcizet, O. *Nature Nanotechnology* **2014,** 9, 920.
7. Roy, S. K.; Sauer, V. T. K.; Westwood-Bachman, J. N.; Venkatasubramanian, A.; Hiebert, W. K. *Science* **2018,** 360, (6394).
8. van Hoorn, C. H.; Chavan, D. C.; Tiribilli, B.; Margheri, G.; Mank, A. J. G.; Ariese, F.; Iannuzzi, D. *Opt. Lett.* **2014,** 39, (16), 4800-4803.
9. Eichenfield, M.; Chan, J.; Camacho, R. M.; Vahala, K. J.; Painter, O. *Nature* **2009,** 462, 78.
10. Larsen, T.; Schmid, S.; Villanueva, L. G.; Boisen, A. *ACS Nano* **2013,** 7, (7), 6188-6193.
11. Schmid, S.; Wu, K.; Larsen, P. E.; Rindzevicius, T.; Boisen, A. *Nano Letters* **2014,** 14, (5), 2318-2321.
12. Kosaka, P. M.; Pini, V.; Ruz, J. J.; da Silva, R. A.; González, M. U.; Ramos, D.; Calleja, M.; Tamayo, J. *Nature Nanotechnology* **2014,** 9, 1047.
13. Thijssen, R.; Verhagen, E.; Kippenberg, T. J.; Polman, A. *Nano Lett* **2013,** 13, (7), 3293-7.
14. Ramos, D.; Gil-Santos, E.; Malvar, O.; Llorens, J. M.; Pini, V.; San Paulo, A.; Calleja, M.; Tamayo, J. *Sci Rep* **2013,** 3, 3445.
15. Gil-Santos, E.; Ramos, D.; Pini, V.; Llorens, J.; Fernández-Regúlez, M.; Calleja, M.; Tamayo, J.; San Paulo, A. *New Journal of Physics* **2013,** 15, (3).
16. Fan, J. A.; Wu, C.; Bao, K.; Bao, J.; Bardhan, R.; Halas, N. J.; Manoharan, V. N.; Nordlander, P.; Shvets, G.; Capasso, F. *Science* **2010,** 328, (5982), 1135-8.
17. Hentschel, M.; Saliba, M.; Vogelgesang, R.; Giessen, H.; Alivisatos, A. P.; Liu, N. *Nano Letters* **2010,** 10, (7), 2721-2726.
18. Pini, V.; Ramos, D.; Dominguez, C. M.; Ruz, J. J.; Malvar, O.; Kosaka, P. M.; Davis, Z. J.; Tamayo, J.; Calleja, M. *Microelectronic Engineering* **2017,** 183-184, 37-41.
19. Verbridge, S. S.; Parpia, J. M.; Reichenbach, R. B.; Bellan, L. M.; Craighead, H. G. *Journal of Applied Physics* **2006,** 99, (12), 124304.
20. Malvar, O.; Ruz, J. J.; Kosaka, P. M.; Domínguez, C. M.; Gil-Santos, E.; Calleja, M.; Tamayo, J. *Nature Communications* **2016,** 7, 13452.
21. Schopf, C.; Noonan, E.; Quinn, A.; Iacopino, D. *Crystals* **2016,** 6, (9), 117.

22. Brandl, D. W.; Mirin, N. A.; Nordlander, P. *The Journal of Physical Chemistry B* **2006,** 110, (25), 12302-12310.